Aquatic Toxicology 158 (2015) 181–191

Contents lists available at ScienceDirect

Aquatic Toxicology

journal homepage: www.elsevier.com/locate/aquatox

Exposure of *Paracentrotus lividus* male gametes to engineered nanoparticles affects skeletal bio-mineralization processes and larval plasticity

Chiara Gambardella[a,*], Sara Ferrando[b], Silvia Morgana[a], Lorenzo Gallus[b], Paola Ramoino[b], Silvia Ravera[c], Mattia Bramini[d], Alberto Diaspro[e], Marco Faimali[a], Carla Falugi[f]

[a] Institute of Marine Science (ISMAR), National Council of Researches (CNR), Via De Marini 6, 16149 Genova, Italy
[b] Department of Earth, Environment and Life Sciences (DISTAV), University of Genova, Viale Benedetto XV 5, 16136 Genova, Italy
[c] Department of Pharmacy (DIFAR), Biochemistry Lab., University of Genova, Viale Benedetto XV 5, 16136 Genova, Italy
[d] Department of Neuroscience and Brain Technologies, Istituto Italiano di Tecnologia (IIT), Via Morego 30, 16163 Genova, Italy
[e] Department of Nanophysics, Istituto Italiano di Tecnologia (IIT), Via Morego 30, 16163 Genova, Italy
[f] Department of Earth, Environment and Life Sciences (DISVA), Polytechnic University of Marche, Ancona, Italy

ARTICLE INFO

Article history:
Received 19 August 2014
Received in revised form
14 November 2014
Accepted 18 November 2014
Available online 25 November 2014

Keywords:
Biomineralization
Cell migration
Nanoparticles
Paracentrotus lividus
Skeletogenesis
Sperm exposure

ABSTRACT

The aim of this study is to contribute to the understanding of the mechanisms underlying nanoparticle (NP)-induced embryotoxicity in aquatic organisms. We previously demonstrated that exposure of male gametes to NPs causes non-dose-dependent skeletal damage in sea urchin (*Paracentrotus lividus*) larvae. In the present study, the molecular mechanisms responsible for these anomalies in sea urchin development from male gametes exposed to cobalt (Co), titanium dioxide (TiO_2) and silver (Ag) NPs were investigated by histochemical, immunohistochemical and Western blot analyses. *P. lividus* sperm were exposed to different NP concentrations (from 0.0001 to 1 mg/L). The distribution of molecules related to skeletogenic cell identification, including ID5 immunoreactivity (IR), wheat germ agglutinin (WGA) affinity and fibronectin (FN) IR, were investigated by confocal laser scanning microscopy at the gastrula (24 h) and pluteus (72 h) stages.

Our results identified a spatial correspondence among PMCs, ID5 IR and WGA affinity sites. The altered FN pattern suggests that it is responsible for the altered skeletogenic cell migration, while the Golgi apparatus of the skeletogenic cells, denoted by their WGA affinity, shows different aspects according to the degree of anomalies caused by NP concentrations. The ID5 IR, a specific marker of skeletogenic cells in sea urchin embryos (in particular of the msp130 protein responsible for Ca^{2+} and Mg^{2+} mineralization), localized in the cellular strands prefiguring the skeletal rods in the gastrula stage and, in the pluteus stage, was visible according to the degree of mineralization of the skeleton. In conclusion, the present study suggests that the investigated NPs suspended in seawater interfere with the bio-mineralization processes in marine organisms, and the results of this study offer a new series of specific endpoints for the mechanistic understanding of NP toxicity.

1. Introduction

Sea urchins are model organisms for the assessment of seawater quality, developmental biology, embryology and bio-mineralization processes (Kobayashi, 1991; Wilt, 2005; Jasny and Prunell, 2006; Siller et al., 2013; Gambardella et al., 2014). Currently, they are successfully used by international agencies for the bio-monitoring and health status assessment of sea coastal environments (USEPA, 2002; ASTM, 2004; Pinsino et al., 2008). *Paracentrotus lividus* is emerging as a valid tool for studies in marine ecotoxicology (Matranga and Corsi, 2012). Because both the gametes and embryos of *P. lividus* are affected by chemicals and xenobiotics dispersed in seawater, several laboratories are currently proposing this alternative and ethical model for the standardization of ecotoxicity tests to identify the noxious

* Corresponding author. Tel.: +39 0106475429.
E-mail addresses: chiagamba@gmail.com, chiara.gambardella@ge.ismar.cnr.it (C. Gambardella).

http://dx.doi.org/10.1016/j.aquatox.2014.11.014
0166-445X/

effects of environmentally relevant contaminants (Buznikov et al., 2001; Qiao et al., 2003; Aluigi et al., 2008; Faimali et al., 2012; Privitera et al., 2012; Siller et al., 2013). In addition, this species has been recently proposed as a model for investigating the effects of nanoparticles (NPs) in seawater (Falugi et al., 2012; Manno et al., 2012; Gambardella et al., 2013; Manzo et al., 2013; Siller et al., 2013). Knowledge of the effects of NPs on marine organisms is scarce. To date, studies on the impact of NPs at the level of the organism primarily use bivalves (*Mytilus galloprovincialis*, Canesi et al., 2010a,b; Zuykov et al., 2011; Barmo et al., 2013; D'Agata et al., 2014), but interest in sea urchins as a model is growing.

Engineered NPs are increasingly produced and employed in many commonly used commercial products, but their possible toxic effects are not fully understood. Recent studies report that they can impair numerous important biological processes, including development and skeletogenesis (Gambardella et al., 2013; Siller et al., 2013). The latter process is critical, especially during its early stages, when skeleton development is genetically programmed. Skeletal formation is a central event in sea urchin morphogenesis because it is essential for larval survival and, therefore, the continuation of the sea urchin population (Decker and Lennarz, 1988). The skeleton of sea urchin embryos is formed by migration of primary mesenchyme cells (PMCs), after which the larvae start feeding and additional arms develop (Yajima and Kijimoto, 2006).

PMC ingression is the earliest recognizable morphogenetic event of gastrulation in sea urchin embryos (Fink and McClay, 1985). The chemistry of the PMCs changes as they move from the wall of the blastula into the blastocoel, following a distinct pattern prior to and during spicule formation (Okazaki, 1975). In this process, PMCs release a glycoprotein from the Golgi apparatus which functions as a center of crystallization of $CaCO_3$ and, in small part, of Mg^{2+}, giving rise to the skeletal rods (Ettensohn and McClay, 1986; Wilt, 1999). A complex series of inputs and genetic responses driving these processes has been identified (McClay et al., 2000). In this interaction between signaling molecules and genetic responses, signals coming from the contaminated environment may interfere with the signal transduction chain (Pesando et al., 2003; Aluigi et al., 2005). For example, disruption of early skeletal pattern formation can be induced either by NPs ingested with food (Gambardella et al., 2014) or as a secondary effect after sperm exposure to different concentrations of cobalt (Co), titanium dioxide (TiO_2) and silver (Ag) NPs (Gambardella et al., 2013).

In the present work, *P. lividus* sperm was exposed to the same NPs at the same concentrations (0, 0.0001, 0.001, 0.01, 0.1 and 1 mg/L) as previously described (Gambardella et al., 2013) and used to fertilize eggs maintained in standard seawater. Histochemical and immunohistochemical analyses of molecules involved in the deposition of skeletal matrix and PMC migration were used to elucidate the mechanisms by which NPs interfere with the correct deposition of the organic matrix, as well as of the molecules responsible for the uptake/deposition of inorganic calcium compounds. We also investigated the fibronectin (FN)-like pattern by using immunohistochemistry and Western blot analysis, along which migrating cells move *via* interactions with integrins located in the glycocalix. In addition, we investigated the affinity sites of the lectin wheat germ agglutinin (WGA, with known affinity to the *N*-acetyl glucosamine and sialic acid oligosaccharide terminals). WGA is a recognized bi-univocal marker of PMCs, as demonstrated by Ettensohn and McClay (1987). We also identified the PMCs by their immunoreactivity (IR) and Western blot analysis to the ID5 antibody specificity (Miller et al., 1995). ID5 is the antibody that recognizes a cell surface antigen, msp130, which is specific for PMCs in the early developmental stages of the sea urchin *P. lividus* and *Strongylocentrotus purpuratus* (McClay et al., 1983; Anstrom et al., 1987; Leaf et al., 1987; Mann et al., 2010; Ettensohn, 2014). The msp130 is a sulfated cell-surface glycoprotein that has been implicated in calcium uptake or deposition in sea urchin skeletogenesis (Carson et al., 1985; Guss and Ettensohn, 1997). In this paper, ID5 antibody was used to identify the skeletogenic cells (PMCs), which express msp130 protein. The features and the morphology of the affinity sites for the lectin and the IR against the proteins were investigated by analyzing their relationships with PMC patterns by confocal laser scanning microscopy (CLSM). Possible alterations of the key molecules responsible for PMC function during skeletogenesis were investigated to establish new, rapid markers of nanotoxicity in the marine environment.

2. Materials and methods

2.1. Nanoparticles characterization

TiO_2 and Co NPs were provided in powder form by NanoAmor (US) with at least 98% purity. Nominal particle sizes were 10–30 nm and 28 nm for TiO_2 and Co, respectively. Ag NPs were obtained from Polytech (WM 1000-c, Germany) and supplied as a suspension at 1000 ppm in deionized water of metallic Ag with a declared NP size between 1 and 10 nm. All NPs were characterized for size and effective surface charge (ζ-potential). Prior to each measurement, TiO_2, Co and Ag NPs were resuspended in ultrafiltered (0.22 μm Teflon filter) seawater (FSW, 37‰ salinity) for size characterization and in distilled water for measuring the effective surface charge at a concentration of 100 mg/L, and sonicated for 15 min using Branson 2510 bath sonicator (Branson Ultrasonic, Danbury, CT, USA).

Size characterization of the NPs dispersed in FSW was determined by Dynamic Light Scattering (DLS) using a Malvern Zetasizer nano ZS (Malvern Instruments Ltd., Worcester- shire, UK). The measurements were conducted at 25 °C by transferring 1 mL of the stock solution to a square cuvette for DLS analysis. A 50 mW laser with a wavelength of 638.2 nm was used as the light source and the measurements were recorded at a detection angle of 173° (backscatter). The same measurements were also repeated after 1 h, in order to detect the presence of agglomerates in FSW.

The ζ-potential of the NPs was measured using a Malvern Zetasizer nano ZS (Malvern Instruments Ltd., Worcestershire, UK). The measurements were conducted at 25 °C by transferring 1 mL of the stock solution to a square cuvette for ζ-potential measurements.

2.2. Samples and sperm exposure

Mature specimens of *P. lividus* were obtained from the hatchery of Camogli (CNR, Genova, Italy), where they were maintained in FSW and were brought to the laboratory according to Amemiya (1996). The spawning of gametes was obtained as previously described (Gambardella et al., 2013) using oral administration of 1:1000 acetylcholine in FSW. The eggs were collected in standard FSW, while the sperm were collected "dry" directly from the genital pores and maintained in aliquots of 200 μL at $T = 4$ °C. Sperm from 3 different specimens were mixed. The experiments were repeated 4 times during the breeding season and were carried out in triplicate.

For the assay, 10 μL of "dry" sperm were exposed to the NP suspensions at serial concentrations (0.0001, 0.001, 0.01, 0.1 and 1 mg/L) per 1 h by adding 1 mL of the NP suspensions to the Eppendorf vials. Negative controls were performed by adding 1 mL of standard FSW. After 1 h, 10 μL of the sperm from each vial were added to multiwell capsules containing approximately 300 eggs/mL in 10 mL standard FSW (pH 8.1). Egg activation occurs within 60 s of the addition of sperm. As little or no effect was found on sperm fertilizing ability, the fertilized eggs were allowed to develop at 18 °C in a thermostatic room and were sampled at 24 and 72 h, corresponding to gastrula and pluteus stages, respectively.

For brevity, we use the term "exposed samples" for the larvae obtained from eggs fertilized by sperm exposed to the NPs and indicate the exposure of sperm with the term "treatment" or "exposure". Thus, the term "exposed gastrulae/plutei" means "gastrulae/plutei obtained from eggs fertilized by exposed sperm".

2.3. Fixation

Gastrula and pluteus stage embryos were fixed with 2% paraformaldehyde in FSW for 10 min at room temperature and prepared for microscopic analyses. The embryos and larvae were rinsed in 0.1 M PBS (pH 7.4), permeabilized by cold methanol and 20% polyethylene glycol (Sigma, Italy) and subsequently rehydrated for histochemical and immunohistochemical reactions.

2.4. Stainings

2.4.1. WGA-affinity sites

WGA is a conventional trans-Golgi marker. In sea urchins, such as *Strongylocentrotus purpuratus* and *P. lividus*, WGA is a recognized bi-univocal marker of PMCs, as demonstrated by Ettensohn and McClay (1987). In addition, it is currently used in a number of models, from protists (Ramoino, 1997) to vertebrates (Karlsson, 1999) to identify the oligosaccharide terminals of glycoproteins contained in the trans-Golgi vesicles. After fixation and rinsing/rehydration in the physiological solution (Tyr, Tyrode, 1910), control and exposed gastrulae and plutei were incubated in the dark for 50 min at room temperature in 0.1 mg/mL WGA directly conjugated to the green fluorochrome Alexa 488 (Molecular Probes, Invitrogen Corporation, USA) diluted 1:800 in PBS. Specificity control was obtained by pre-incubating the samples with 1:1000 neuraminidase (Sigma, Italy).

2.4.2. Fibronectin-like immunoreactivity

Control and NP-exposed samples were incubated overnight in a moist chamber at 4 °C with the primary rabbit polyclonal antiserum to FN (Dako, Denmark). The antiserum was diluted 1:200 in PBS (pH 7.4) with 0.1% bovine serum albumin (BSA). The negative control was performed by omitting the primary antiserum. After incubation, samples were rinsed in PBS and incubated for 2 h at room temperature in the secondary anti-rabbit Alexa 488 (1:800 in PBS, Molecular Probes, Invitrogen Corporation, USA). All samples were thoroughly washed in PBS, counterstained with propidium iodide (PI) as previously described and mounted on slides with the antifading agent Gelvatol (Lennett, 1978) for microscopic observations.

2.4.3. ID5 immunoreactivity

For ID5 immunofluorescence, embryos were fixed for 20 min in methanol at −20 °C. They were incubated with the monoclonal antibody as described by Miller et al. (1995). This was followed by incubation in the secondary goat anti-mouse IgG, diluted 1:100 in PBS and conjugated with Alexa 488.

These antibodies have been obtained from David McClay (anti-*S. purpuratus*) and from Jenifer Croce (anti-*P. lividus* msp130 PMC surface antigen). In this work, both antibodies were used with similar results.

2.4.4. Nuclear counterstaining

All the stained samples were rinsed in the physiological solution (Tyr for WGA; PBS for immunoreactions), DNA was stained for 15 min at room temperature in 4% PI (Life Technologies, USA) in Tyr. Pre-incubation in 10^{-3} M RNAse A (Sigma, USA) was performed for 20 min at room temperature to avoid RNA staining.

2.5. Microscopy and imaging

Some embryos and larvae were embedded in paraffin and cut in 5 μm thick sections according to the current methods before being stained and mounted in Gelvatol. Most embryos were pre-stained and mounted *in toto* for the 3D confocal laser scanning microscopy (3D CLSM). Images (1024 × 1024 × 8 bit) were acquired on a Leica TCS SP5 AOBS CLSM (Leica Microsystems Mannheim, Germany), using a one Airy disk unit pinhole diameter and an HCX PL APO 40 x/1.25 oil immersion objective. Magnifications were obtained by scan field selection. Alexa Fluor 488 was excited with the 488 nm line of an Ar laser, and the resulting fluorescence was collected in a spectral window of 500–530 nm. PI was excited with the 543 line of the He–Ne laser, and the fluorescence of this dye was collected in a spectral window of 600–640 nm. Laser scanning transmitted light images were obtained using the 488 nm laser line. The Leica Confocal Software program was used for image acquisition, storage and analysis.

2.6. Western blot analysis

Controls were frozen at −80 °C and used for Western blot analysis. Denaturing electrophoresis (SDS-PAGE) was performed using Laemmli protocol on gradient 10–15% acrylamide gels (Laemmli, 1970). Sea urchins larvae were homogenated in PBS and sonicated for 10 s twice times, at 4 °C. For each sample, 30 μg of total protein were loaded. The run was performed at 4 °C and at 70 mA. After blot, nitrocellulose membrane were labeled with the following primary antibodies diluted in PBS: mouse Ab against ID 5, diluted 1:200 in PBS with 0.05% Tween 20 (PBSt) 0,15%, and rabbit anti-FN, diluted 1:600 in PBSt 0.15%. Secondary HPR-conjugated Ab_s were diluted 1:10,000 in PBSt 0.15%. Bands were visualized by chemiluminescence with Immuno-Star WesternC kit (BioRad Lab, Hercules, CA) and images were acquired with the molecular imager ChemiDoc XRS+ System (Bio-Rad). The molecular weight of the signals was calculated using the ChemiDoc XRS+ System software. Protein concentration of the samples was determined by Bradford method, using BSA as a standard protein (Bradford, 1976).

2.7. Statistics

Currently, it is impossible to know how many NPs may contact the organisms without penetration for each known concentration of NPs in seawater. Although NPs are applied in suspension, it is difficult to predict their behavior due to their tendency to clump together in the aquatic medium. Therefore, the statistical analysis of data was made using an "odds ratio" and "relative risk" (RR) calculation that is used for epidemiological studies where the environmental conditions are not fully established.

3. Results

3.1. Characterization of NPs

The results of NP characterization are summarized in Table 1 and Supplementary Table 1, reporting size and ζ-potential of each NP. The characterization, especially under the conditions in which the NPs will be presented to the sperm (in FSW, 37‰ salinity for 1 h), is essential in order to understand the dose of NPs that is being presented to the sperm, as significant agglomeration of the NPs in the FSW would reduce the available NP dose. The data in Table 1 and Supplementary Table 1 highlight a key limitation of the DLS technique, that it gives a mean value, which is physically quite meaningless in the presence of multiple peaks such as are observed here. However, for the purpose of our study, the understanding of

Table 1
Physicochemical characterization of the NPs used in the study. NP size and ζ-potential analysis are referred to FSW and distilled water, respectively. Due to high poly-dispersity index (PDI), the values and percentage of peak 1 and peak 2 are reported. DLS and ζ-potential results are the average of a minimum of three separate runs; errors represent the standard deviation over measurements and are intended solely as an indication of the reproducibility of the measurement.

Sample	T (°C)	Diameter[a] (nm)	PDI[b]	Peak 1	Peak 2	ζ-Potential (mV)
TiO_2 NPs	25	652	0.38	563 ± 180 (97%)	5264 ± 451 (3%)	−12 ± 4
Co NPs	25	918	0.54	556 ± 111 (100%)	–	−17 ± 12
Ag NPs	25	990	0.80	324 ± 53 (68%)	151 ± 11 (32%)	−3 ± 2

[a] *z*-Average hydrodynamic diameter extracted by cumulant analysis of the data.
[b] Polydispersity index from cumulant fitting of the data.

the NP solutions in FSW over time was necessary and the DLS analysis showed a shift in apparent particle size after 1 h, suggesting an increase of agglomeration (Supplementary Fig. 1).The ζ-potential of both TiO_2 and Co NPs was negative, while the ζ-potential of Ag NPs tended to neutrality.

3.2. Morphology

The morphological results confirmed the skeletal anomalies and their rates, which were previously reported by Gambardella et al. (2013). The exposed samples differed from the controls, particularly in the alteration of the skeletogenic pattern and cell death. The latter was not followed by embryonic and larval death, but left naked skeletal structures at the tip of the arms and the distal tip of the hood. The percentage of anomalies varied among the NPs and their concentrations but not in a dose-dependent way, as demonstrated by the low R^2 value in Fig. 1, except for Ag NPs ($R^2 = 0.98$). The highest risk of skeletogenic anomalies was displayed by samples exposed to TiO_2 NPs and to Ag NPs. Exposure to Co NPs resulted in a lower frequency of larvae with anomalous arrangement of the spicules (Fig. 1), at every concentration. At the highest concentrations of each NP, other severe anomalies were preeminent, so that the rate of skeletal defects appeared lower (*e.g.*, exposure to 1 mg/L).

3.3. Gastrula stage

3.3.1. WGA affinity

Control gastrulae PMCs exhibited positive WGA staining at the cell surface and in the matrix deposited at their bases (Fig. 2a and b). The identified cells formed a ring around the blastopore, the site of their ingression. Two strands of cells from this ring projected toward the top of the blastocoel, and at their intersection with the basal ring the first tridimensional axes of the skeletal rods were formed and mineralized (Fig. 2c and d).

In controls, the ectoderm displayed a continuous epithelial structure formed by tight cells. WGA affinity sites were present in inner cells, identified as PMCs by the green WGA staining of fluorescein isothiocyanate conjugated with the lectin (Fig. 2a and b) and by the presence of ID5 immunoreactivity (Fig. 3a–d). Fluorescence in WGA-labeled cells was located inside the cytoplasm and at the surface of the control gastrulae. The stained structures appeared as a ribbon joining the adjacent cells, with small positive vesicles entering the common cytoplasmic structures (Fig. 2d: the vesicles are indicated by arrows). In contrast, the gastrulae exposed to TiO_2 NPs exhibited a loose arrangement of the ectodermal cells and a different architecture of the PMC cytoplasm: these cells did not show a continuous cytoplasm schema, but the deposited materials were present in the form of granules (Fig. 2e and f). The gastrulae exposed to different doses of Ag NPs also differed from controls, but in a similar manner among the different concentrations (Fig. 2g). The gastrula stage appeared almost normal, but the WGA-labeled cytoplasmic vesicles were retained inside the cytoplasm, appearing round with no stained extensions (Fig. 2g and h). The gastrulae exposed to the lower concentrations of Co NPs (0.001 and 0.0001 mg/L) were similar to controls (not shown), but presented skeletal anomalies at the later stages (Fig. 5). The gastrulae exposed to the higher concentrations of Co NPs (0.01–1 mg/L) exhibited a disaggregation of all the body cells and irregular distribution of WGA affinity sites, which formed tiny dots inside all or part of the cytoplasm (Fig. 2i).

3.3.2. ID5 immunoreactivity

In control gastrulae, the ID5 antibody reacted with the PMCs and labeled the surface of PMCs and the matrix at their bases. The pattern of the skeletogenic cells was the same as that revealed by WGA (Fig. 3a–i). The gastrulae obtained from exposure to 0.01 mg/L Ag NPs did not differ greatly from the controls (Fig. 3a, b, d and e), while

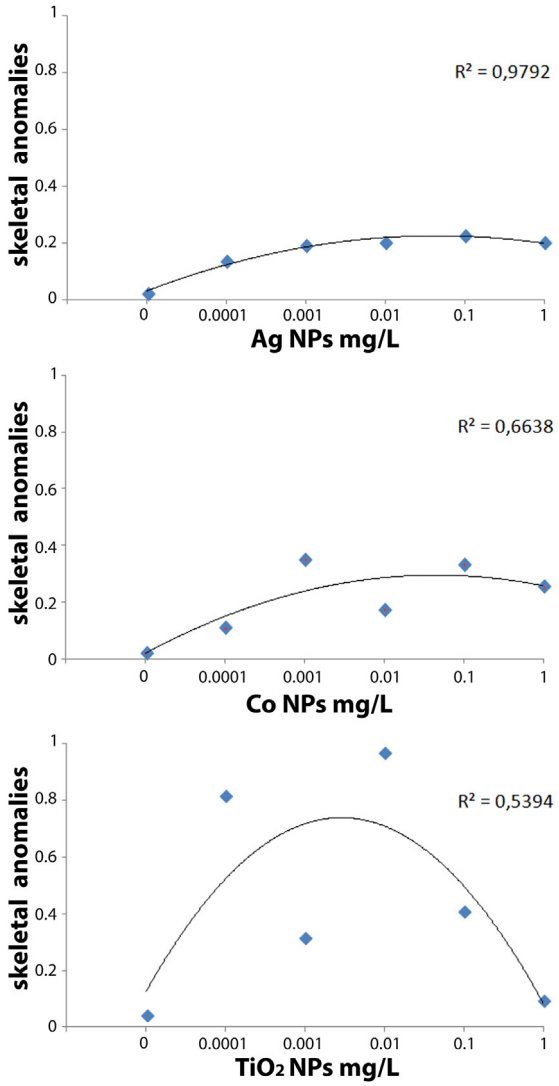

Fig. 1. Probability of skeletal anomalies in larvae obtained from sperm exposed to the different NPs (risk ratio).

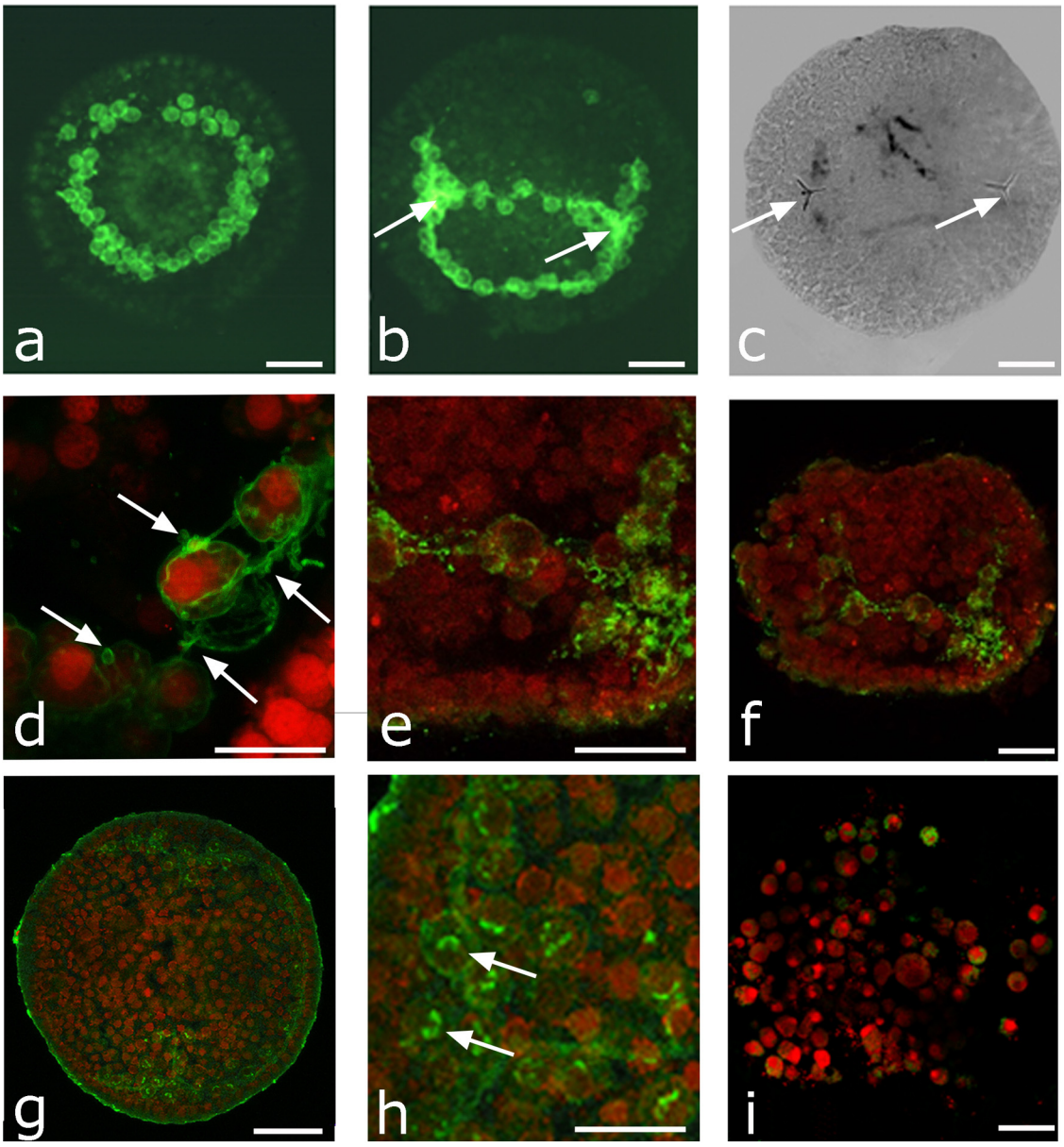

Fig. 2. CLSM images of WGA affinity sites (green fluorescence). (a–d) Control gastrula. (a) Gastrula view from the blastopore side; (b and c) gastrula view from lateral side. The arrows indicate the first skeletal rods. (d) High magnification of a gastrula stage, showing the continuity of cytoplasm and the Golgi vesicles (arrows). (e and f) Gastrulae from sperm exposed to TiO_2 NPs (0.01 mg/L). (g and h) Gastrula obtained from sperm exposed to Ag NPs (0.01 mg/L). (i) 5 μm paraffin section of a gastrula from sperm exposed to Co NPs (0.01 mg/L). (d–i) Nuclei were counterstained by PI (red fluorescence). (a–c, f, g and i) Bars = 50 μm; (d, e and h) bars = 10 μm. (For interpretation of the references to color in this figure legend, the reader is referred to the web version of this article.)

the gastrulae exposed to higher concentrations showed ID5 pattern anomalies, as did those exposed to TiO_2 NPs. An example of a gastrula exposed to 0.01 mg/L TiO_2 NPs is shown (Fig. 3c, f and g). The most severe anomalies resulted from exposure to 1 and 0.1 mg/L NPs. The ID5 IR image shown is from exposure to Co NPs (Fig. 3h and i), taken from a section contiguous to the one represented in Fig. 2i.

3.3.3. *FN-like immunoreactivity*

The deposition of FN-like molecules exhibited the same pattern in controls (Fig. 4a) and in embryos exposed to the lower NP concentrations (Fig. 4b), while it was perturbed and irregular in the gastrulae obtained from exposure to the high concentration. The example in Fig. 4c refers to 0.01 mg/L TiO_2 NPs. Histological sections of controls revealed the distribution of FN-like IR over the blastocoel walls and at the surface of the migrating cells (Fig. 4d).

3.4. *Pluteus stage*

Here, we show the morphological and immunohistochemical features of the larvae that survived to the 72 h pluteus stage.

Among all the samples exposed to the different NPs, the skeletal anomalies were neither homogeneous nor dose-dependent (as previously described by Gambardella et al., 2013, 2014) but generally were represented by joined, asymmetrical or missing perioral arms (caused by all the NPs, Scheme 1, Fig. 5j, l, i and m) and by crossed skeletal rods at the end of body (primarily from Ag and Ti exposures, Fig. 5e, j and k). In addition, exposure to TiO_2 NPs at

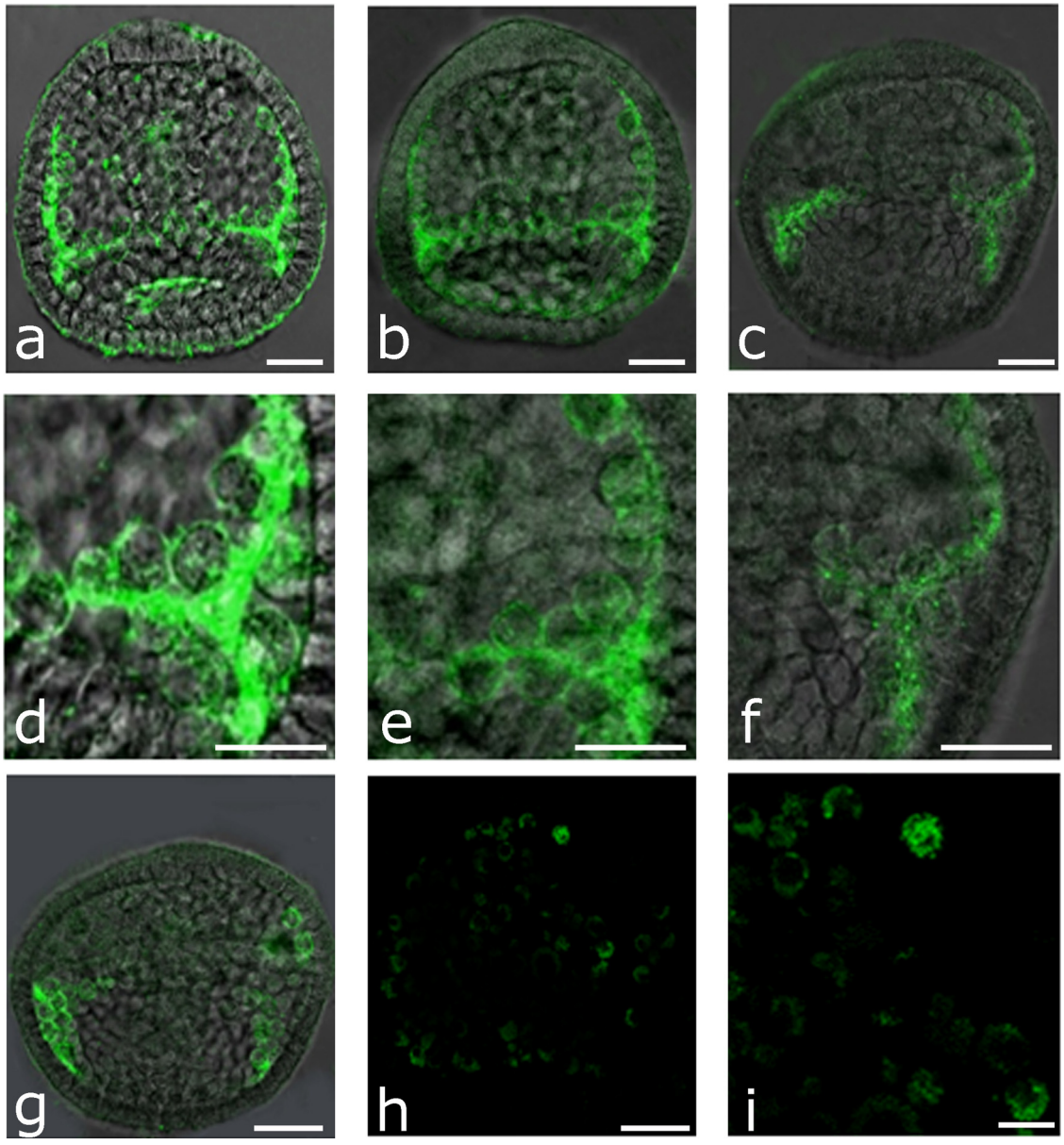

Fig. 3. CLSM images of ID5 IR. (a and d) Control gastrula. ID5 IR is present at the cell surface and over the skeletal structures. (b and e) IR in gastrulae obtained from sperm exposed to 0.01 mg/L Ag NPs. (c, f and g) IR in gastrulae obtained from sperm exposed to 0.01 TiO_2 NPs. (h and i) IR from exposure to 0.01 mg/L Co NPs (histological sections). (a, c and i) Bar = 50 μm; (d–f) bar = 10 μm; (g and h) bar = 30 μm.

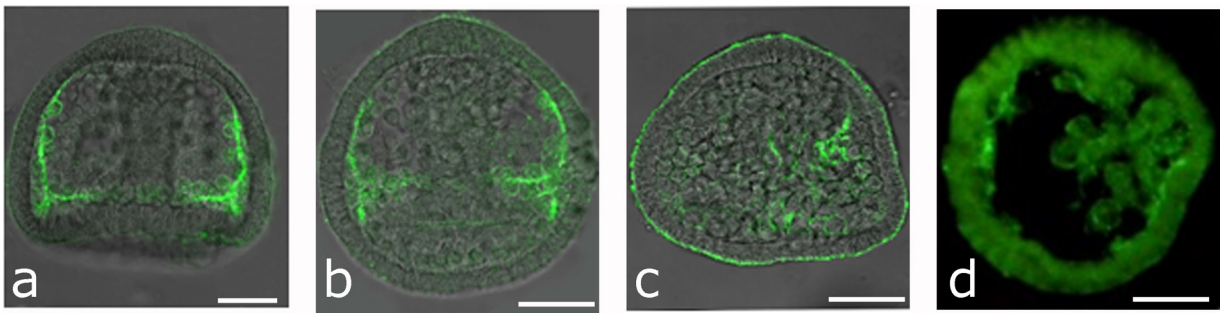

Fig. 4. CLSM images of FN IR. (a) IR in control gastrula; (b) FN IR in gastrula exposed to 0.01 mg/L Ag NPs; (c) FN IR in gastrula exposed to 0.01 mg/L TiO_2 NPs. (d) FN IR in histological sections of a control early gastrula, 5 μm paraffin section. Bar = 50 μm.

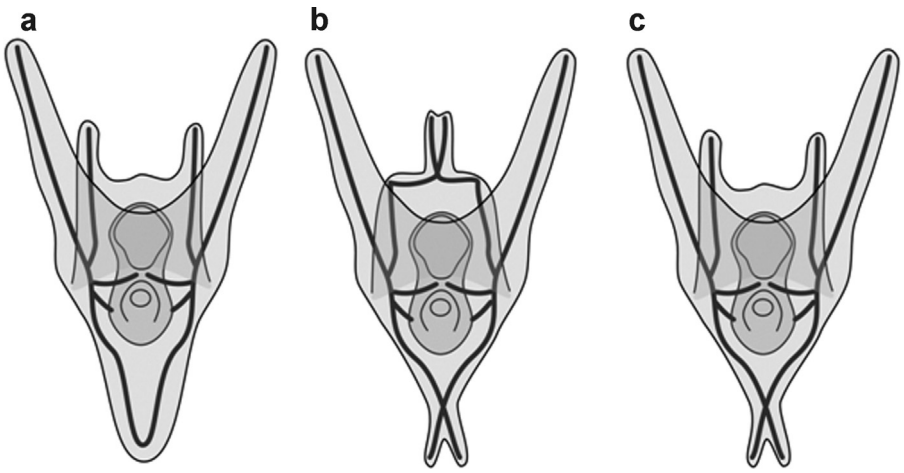

Scheme 1. Main skeletal anomalies found in treated plutei compared to control. (a) Control pluteus, (b) pluteus with joined anterior perioral arms and crossed distal skeletal rods, typical of samples exposed to Co NPs; (c) pluteus with crossed distal skeletal rods, primarily found in samples exposed to TiO_2 NPs.

every concentration caused a percentage of larvae to demineralize, identified by the presence of tiny rods and fragility, *i.e.* being easily broken by gentle handling (Fig. 5g and m).

3.4.1. WGA affinity

The control larvae exhibited organized skeletal matrix, surrounded by adherent cells. As previously described in PMCs, the substance released by the Golgi vesicles formed a subtle layer at the surface of the skeletal rods (Fig. 5a, b and e). The exposure to TiO_2 affected plutei, as the trans-Golgi vesicles did not appear sharply defined. In some cases, the positive cells appeared far from the skeletal spicules, losing connection with them (Fig. 5c and d). The skeletal rods appeared discontinuously coated with the fluorescent matrix.

In the samples exposed to the other NPs and exhibiting skeletal anomalies, the WGA IR material was closely packed in the trans-Golgi vesicles (Fig. 5g–j, l and m: related to the exposure to Ag NPs) except in the samples with demineralized and fragile skeletal rods (Fig. 5f, Ag 0.001 mg/L). Here, the trans-Golgi vesicles were strongly WGA-positive, whereas in the controls, no IR was observed on the skeletal rods, and the trans-Golgi vesicles were retained inside the cytoplasm (Fig. 5e). The cytoplasm of these cells closely contacted the damaged rods, and the Golgi vesicles appeared oriented toward the skeletal rods.

In plutei exposed to Co 0.01 mg/L, the WGA-positive cells resembled cells in plutei exposed to TiO_2: the Golgi vesicles were transparent, and the WGA-positive matrix formed a thin layer over the spicule (Fig. 5n). Exposure to 0.1 mg/L Co (Fig. 5k) caused more severe anomalies, and in this case the Golgi vesicles were arranged similarly to the one shown in Fig. 5f.

3.4.2. ID5 immunoreactivity

ID5 IR in plutei followed the distribution pattern of the WGA-positive cells, but not as closely as in the gastrula stage (Fig. 6 refers to 72 h plutei). Additionally, the presence of staining over the spicules was discontinuous, except for the subtle skeletal rods of the larvae obtained from exposure to 0.01 mg/L TiO_2 NPs (*e.g.*, Fig. 5d, arrow).

3.4.3. FN-like immunoreactivity

Fibronectin-like immunofluorescence (Fig. 7) followed a similar pattern as PMC distribution as revealed by WGA staining and ID5 IR.

3.5. Western blot

Western blot analysis, based on control larvae homogenate, are consistent with the immunohistochemical results, showing signal bands with molecular weight around 262 kDa for FN and 52 kDa and 130 kDa for ID5 (Fig. 8). In this case the two bands corresponded to the msp130 proteins while the second one could correspond to another protein recognized by the ID5 antibody.

4. Discussion

4.1. Possible interactions of NPs in sea urchin gametes

In all cases, responses to NP exposure were present, and damage to the embryos and larvae was exhibited. The sharp difference between control and exposed samples indicates that the observed damage resulted from the presence of NPs. The fact that the exposed samples did not differ in a dose-dependent manner suggests that different parameters, such as NP size or shape, are involved that are more important than NP concentration. Here, we demonstrated that the size of all the used NPs in seawater is higher than the nominal one provided by the commercial companies and that the size increases along the short exposure time (1 h). The effective size of NPs is an important parameter to consider in the pathway selection of NPs entry into cells. The huge aggregates found in all NP suspensions may prevent the internalization of NPs through the cell membrane and it is understandable that the small particles may be beneficial to enter the cells rapidly (Huang et al., 2002). Therefore, the effect exerted by the most diluted NPs may actually be more specific because the rare particles have a low chance of interacting one with each other and forming clusters, as we demonstrated by the physicochemical characterization. In this way, they remain small in size, allowing them to enter the cells. The effect of the most concentrated NPs may be due to their crowding on the cells surface and forming structures.

In addition, effective surface charge results highlight the negative ζ-potential of TiO_2 and Co NPs, whereas Ag NPs tended to neutrality. For this reason, TiO_2 and Co NPs may need a carrier in order to be transferred inside the cells through, for example, endocytic processes. Although endocytotic vesicles, such as clathrin-coated vesicles, have a physiological diameter of $\approx$100 nm, they have been demonstrated to contain NPs of a size ranged from 10 nm to 500 nm and limited to 5 μm (Kou et al., 2013). The neutral Ag NP effective surface charge may instead allow a different

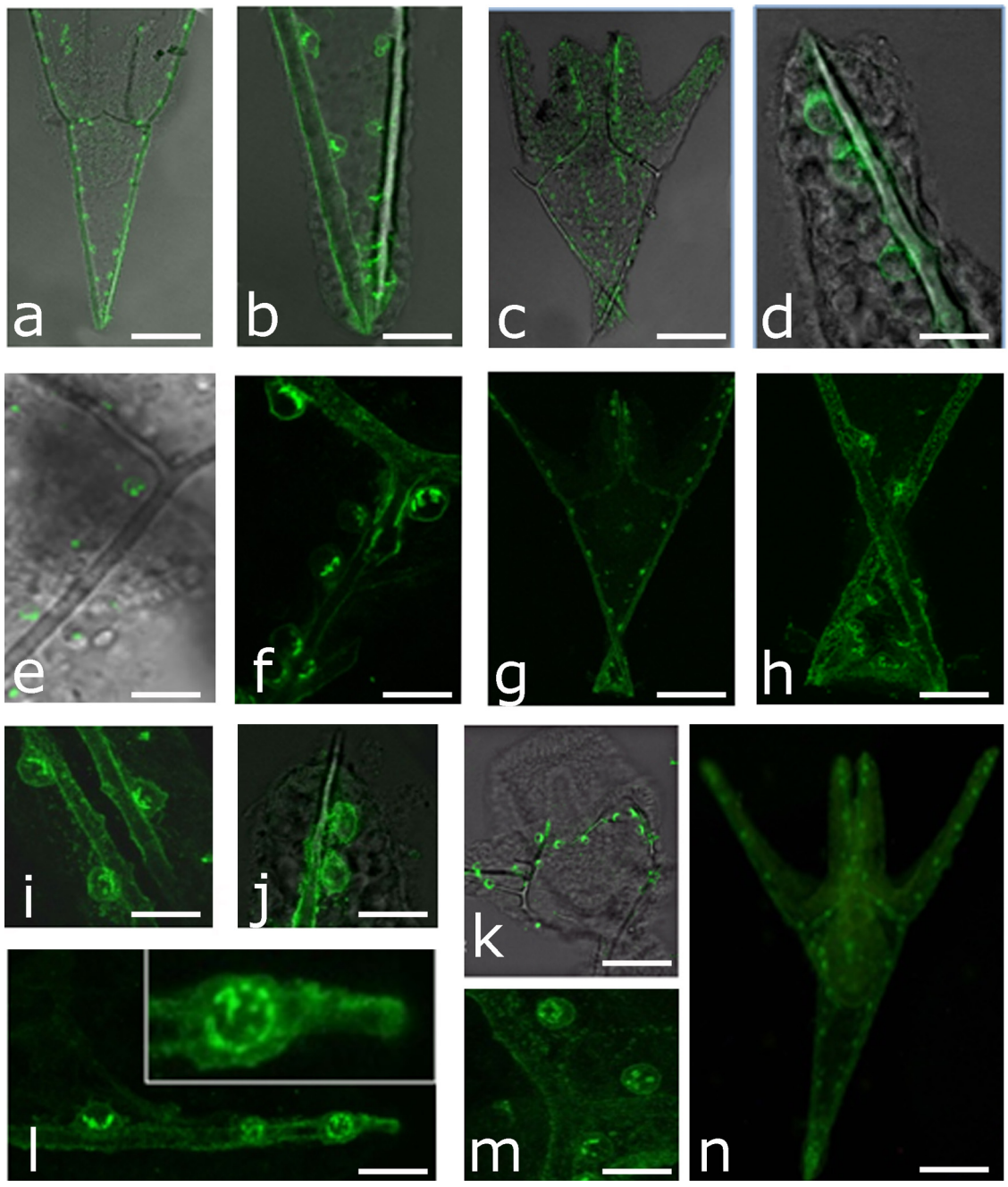

Fig. 5. CLSM images of WGA affinity sites (green fluorescence). (a, b and e) Control plutei; (c, d and f) plutei exposed to TiO_2 NPs; (g–j, l and m) plutei exposed to Ag NPs; (k and n) plutei exposed to Co NPs. (c, d and f) Plutei exposed to 0.01 mg/L TiO_2 NPs; (g) pluteus exposed to Ag NPs 0.1 mg/L. (h) Higher magnification of (g). (i, j and m) Ag NPs 0.001; (k) 0.1 mg/L Co NPs. (l) Ag NPs 0.01 mg/L. (n) 0.01 mg/L Co NPs. (a, c, g, k and n) Bar = 50 μm. (b, d, e, f, h, i, j, l and m) Bar = 25 μm.

NP uptake mechanism, such as passive passage through the apolar lipids of the cell membranes.

The size and effective surface charge are in agreement with the histochemical and immunohistochemical results and can explain the toxicological mechanisms underlying the bio-mineralization process alteration in sea urchin early developmental stages.

4.2. Morphology and formation of skeletal rods

Many proteins that form the organic matrix of the skeletal rods are expressed by the PMCs. The latter may be identified by their affinity to WGA that marks the Golgi apparatus of these cells. NP exposure specifically affects the WGA-positive Golgi apparatus.

These results indicate that exposure of sperm to different NPs affects the patterning of skeletal structures by interfering with the expression of molecules responsible for PMC migration, the performance of the PMC Golgi apparatus in organic matrix deposition and the expression of the msp130 surface protein.

These anomalies have previously been classified and their frequency has been reported in samples exposed to the same NPs at the same concentrations used here (Gambardella et al., 2013) and have been proposed as specific biomarkers of stress for *P. lividus* model (Carballeira et al., 2012).

The presence and takeover of WGA-positive molecule deposition shows that the constructive phase of the skeletal matrix is a continuous process during development of the plutei. This is also shown by the presence of ID5 IR, which recognizes the msp130

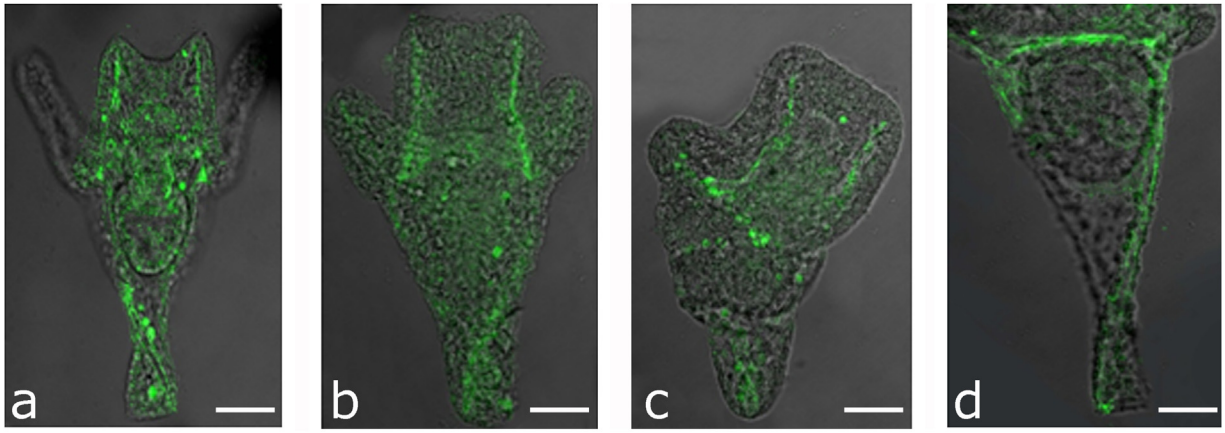

Fig. 6. *P. lividus* 48 h plutei. Immunoreactivity to ID5 (green fluorescence): (a) exposure to Ag NPs 0.001 mg/L; (b) exposure to Ag NPs 0.01 mg/L; (c) exposure to Ag NPs 0.1 mg/L; (d) exposure to 0.01 mg/L TiO_2 NPs. Bars = 50 μm. (For interpretation of the references to color in this figure legend, the reader is referred to the web version of this article.)

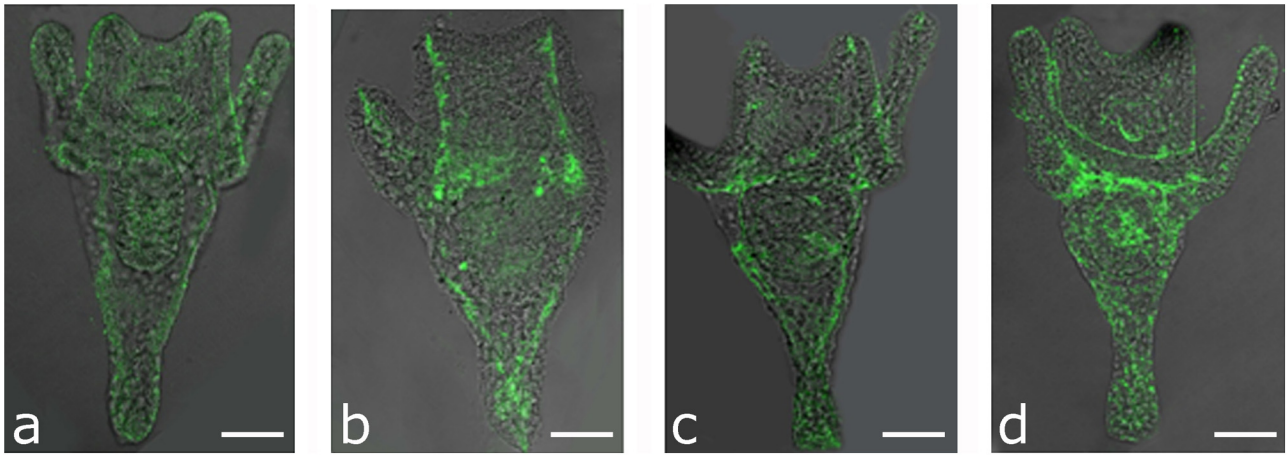

Fig. 7. Images of *P. lividus* 48 h larvae. FN-like IR: (a) exposure to 0.001 mg/L Ag NPs; (b and c) exposure to 0.01 mg/L Ag NPs; (d) exposure to 0.01 mg/L TiO_2 NPs. Bar = 50 μm.

surface antigen, which performs calcium uptake and deposition. According to the literature (McClay et al., 1983; Leaf et al., 1987), the ID5 IR gradually disappears after the gastrula stage. However, after exposure to NPs, we found that the IR persisted in damaged skeletal rods. This may contribute to healing of the anomalous demineralized skeleton, with a continuous action ensuring echinoderm larval plasticity (Fenaux et al., 1994).

The first step of the constructive process is represented by PMC migration. This process may be driven by deposition of molecules immunologically related to FN (Falugi et al., 2008), which occurs in organisms where the cell migration driving gastrulation is due to poly ingression, such as primary and secondary mesenchyme of echinoderms. No FN deposition occurs in organisms where gastrulation movements occur by embolism. Thus, very few reports are available in the literature.

The control gastrulae showed the same FN-like IR distribution pattern as described by Spiegel et al. (1980) on the outer cell surfaces and between cells of the sea urchin embryos during early

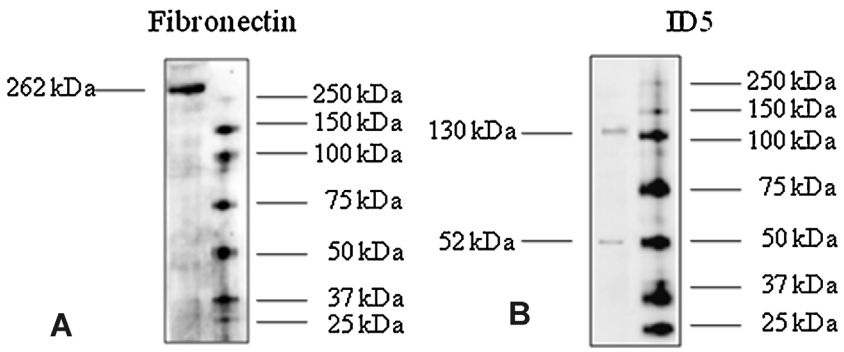

Fig. 8. Western blot detection of FN and ID5 in the control larvae. Panel (A) shows the WB analysis using an antibody against FN, where it is visible a band approximately at 262 kDa. Panel (B) reports the WB analysis using an antibody against ID 5. In this case, two bands are visible, one at ~52 kDa and one at ~130 kDa corresponding to msp130 proteins and to another protein recognized by the ID5 antibody.

development. Functions previously ascribed to FN in vertebrates, such as cell recognition, cell adhesion, cell motility and the mediation of cell-to-cell interactions may now be predicted for this FN-like protein. In vertebrates, FN molecules are strongly linked to cell migration both *in vivo* and *in vitro*. The process is due to the interaction between the glycocalix integrins and the gradient of FN distribution (Johansson et al., 1997). This has also been demonstrated for sea urchin (Katow and Hayashi, 1985; Katow et al., 1990; Susan et al., 2000). During gastrulation, PMCs undergo poly ingression following FN pathways and form the matrix on which calcium carbonate crystallizes to form the skeletal rods (Ettensohn and McClay, 1986; Wilt, 1999). This migration is impaired by exposure to contaminants that generate stress (Pesando et al., 2003). Thus, the localization of FN-like molecules in the skeletogenic pattern of anomalous embryos suggests that interference by NPs in the deposition of extracellular matrices such as FN is a primary cause of erroneous migration. These results are in agreement with findings in other species, including vertebrates, where NPs have been shown to disturb the FN-mediated adhesion and spreading of pre-osteoblastic cells *in vitro* by Bernier et al. (2012).

The described results show an effect of sperm exposure on the early development of sea urchin *P. lividus*. The question of how sperm exposure to NPs affects embryonic development remains open. Based on our results, we can speculate that either the NPs penetrate inside sperm, reaching the nucleus and causing specific mutations, or the NPs absorbed on sperm surface are inserted into the egg. Unlike other organisms, sea urchin sperm cytoplasm, including centrioles, mitochondria and organelles, is injected in its entirety into the egg (Epel, 1978). The sperm membrane is embedded in the egg membrane, as a mosaic tessera. Thus, the absorbed NPs may enter the egg or remain adsorbed on the egg membrane. The sperm is very small compared to the egg surface. However, the NPs may not only be carried by the one fertilizing sperm but also by the others that remain in contact with the egg surface and jelly coat during the early phases of development. The NPs might be released from the sperm to jelly coat and egg membrane due to different adhesive properties and from there penetrate into or be adsorbed onto the egg. This hypothesis might also explain the lack of dose-dependence of the effects, because during fertilization the number of sperm approaching the eggs is not uniform in each bowl.

4.3. Larval plasticity of the sea urchin

Skeleton formation is a central event in sea urchin morphogenesis (Decker and Lennarz, 1988). It is essential for larval survival and, consequently, for the continuity of sea urchin population. In this process, the plasticity of the larvae allows them to build, destroy and rebuild the larval structures according to the environmental conditions. This process has been correlated by several authors (Fenaux et al., 1994) to the availability of food and its energetic content. However, some researchers also showed that it may also be correlated to the effects of contaminants, including environmental changes, acidification (Martin et al., 2011) or, as in this case, exposure to NPs. A continuous process of re-mineralization may be carried out by the persistence of WGA-positive cells, bringing the trans-Golgi vesicles into contact with the skeletal spicules. At the same time, the msp130 surface molecule (demonstrated by the ID5 IR) continues the uptake/deposition of minerals on the matrix surrounding the spicules. This is suggested by the sharp staining of ID5 in the larvae affected by TiO_2 NPs (Fig. 6d).

5. Conclusions

In conclusion, sea urchin larval development is a sensitive model for NP effects, but attention must be paid to the possible masking effects of sea urchin larval plasticity, which may lead researchers to underestimate the effects of exposures as well as the characterization and possible behavior of NPs in seawater.

Our results confirm that simple histochemical and immunohistochemical reactions may constitute easy and fast biomarkers in early embryos or larvae of sea urchins (small, transparent, and easy to handle and to stain *in toto*) in keeping with the recent EU initiative for Reduction, Refinement and Replacement (3Rs) of high vertebrates in toxicological experiments.

Acknowledgments

We thank Prof. David McClay, Dr. Valeria Matranga and Dr. Jenifer Croce for kindly supplying the ID5 antibody. This work was performed in the frame of the INESE project (Impact of Nanoparticles on Environmental Sustainability and Ecology) supported by IIT (Istituto Italiano di Tecnologia, Genova, Italy). Authors also express their sincere thanks to the Nanochemistry Department team of IIT for providing laboratory facilities for NP physicochemical characterization.

Appendix A. Supplementary data

Supplementary data associated with this article can be found, in the online version, at http://dx.doi.org/10.1016/j.aquatox.2014.11.014.

References

Aluigi, M.G., Angelini, C., Falugi, C., Fossa, R., Genever, P., Gallus, L., Layer, P.G., Prestipino, G., Raonczay, Z., Sgrò, M., Thielecke, H., Trombino, S., 2005. Interaction between organophosphate compounds and cholinergic functions during development. Chem. Biol. Interact. 157–158, 305–316.

Aluigi, M.G., Angelini, C., Corte, G., Falugi, C., 2008. The sea urchin, *Paracentrotus lividus*, embryo as a bioethical model for neurodevelopmental toxicity testing. Effects of diazinon on the intracellular distribution of OTX2-like proteins. Cell. Biol. Toxicol. 24, 587–601.

Amemiya, S., 1996. Complete regulation of development throughout metamorphosis of sea urchin embryos devoid of macromeres. Dev. Growth Differ. 38, 465–476.

Anstrom, J.A., Chin, J.E., Leaf, D.S., Parks, A.L., Raff, R.A., 1987. Localization and expression of msp 130 a primary mesenchyme lineage specific cell surface protein of the sea urchin embryo. Development 101, 255–265.

ASTM (American Society for Testing, Materials), 2004. Standard Guide for Conducting Static Acute Toxicity Tests with Embryos of Echinoid Embryos. ASTM (American Society for Testing, Materials), pp. E1563–E1598.

Barmo, C., Ciacci, C., Canonico, B., Fabbri, R., Cortese, K., Balbi, T., Marcomini, A., Pojana, G., Gallo, G., Canesi, L., 2013. In vivo effects of *n*-TiO_2 on digestive gland and immune function of the marine bivalve *Mytilus galloprovincialis*. Aquat. Toxicol. 132–133, 9–18.

Bernier, M-C., Besse, M., Vayssade, M., Morandat, S., El Kirat, K., 2012. Titanium dioxide nanoparticles disturb the fibronectin-mediated adhesion and spreading of pre-osteoblastic cells. Langmuir 28, 13660–13667.

Bradford, M.M., 1976. A rapid and sensitive method for the quantitation of microgram quantities of protein utilizing the principle of protein–dye binding. Anal. Biochem. 72, 248–254.

Buznikov, G.A., Nikitina, L.A., Bezuglov, V.V., Lauder, J.M., Padilla, S., Slotkin, T.A., 2001. An invertebrate model of the developmental neurotoxicity of insecticides: effects of chlorpyrifos and dieldrin in sea urchin embryos and larvae. Environ. Health Perspect. 109, 651–661.

Canesi, L., Ciacci, C., Vallotto, D., Gallo, G., Marcomini, A., Pojana, G., 2010a. In vitro effects of suspensions of selected nanoparticles (C60 fullerene, TiO_2, SiO_2) on *Mytilus hemocytes*. Aquat. Toxicol. 96, 151–158.

Canesi, L., Fabbri, R., Gallo, G., Vallotto, D., 2010b. Biomarkers in *Mytilus galloprovincialis* exposed to suspensions of selected nanoparticles (nano carbon black, C-60 fullerene, nano-TiO_2, nano-SiO_2). Aquat. Toxicol. 100, 168–177.

Carballeira, C., Ramos-Gomez, J., Martin-Diaz, L., Del Valls, T.A., 2012. Identification of specific malformations of sea urchin larvae for toxicity assessment: application to marine pisciculture effluents. Mar. Environ. Res. 77, 12–22.

Carson, D.D., Farach, M.C., Earles, D.S., Decker, G.L., Lennarz, W.J., 1985. A monoclonal antibody inhibits calcium accumulation and skeleton formation in cultured embryonic cells of the sea urchin. Cell 41, 639–648.

D'Agata, A., Fasulo, S., Dallas, L.J., Fisher, A.S., Maisano, M., Readman, J.W., Jha, A.N., 2014. Enhanced toxicity of 'bulk' titanium dioxide compared to 'fresh' and 'aged' nano-TiO_2 in marine mussels (*Mytilus galloprovincialis*). Nanotoxicology 8, 549–558.

Decker, G.L., Lennarz, W.J., 1988. Skeletogenesis in the sea urchin embryo. Development 103, 231–247.
Epel, D., 1978. Mechanisms of activation of sperm and egg during fertilization of sea urchin gametes. In: Moscona, A.A., Monroy, A. (Eds.), Current Topics in Developmental Biology. Academic Press, New York, pp. 185–246.
Ettensohn, C.A., McClay, D.R., 1986. The regulation of primary mesenchyme cell migration in the sea urchin embryo: transplantations of cells and latex beads. Adv. Dev. Biol. 117, 380–391.
Ettensohn, C.A., McClay, D.R., 1987. A new method for isolating primary mesenchyme cells of the sea urchin embryo: panning on wheat germ agglutinin-coated dishes. Exp. Cell. Res. 168, 431–438.
Ettensohn, C.A., 2014. Horizontal transfer of the msp130 gene supported the evolution of metazoan biomineralization. Evol. Dev. 16, 139–148.
Faimali, M., Giussani, V., Piazza, V., Garaventa, F., Corrà, C., Asnaghi, V., Privitera, D., Gallus, L., Cattaneo-Vietti, R., Mangialajo, L., 2012. Toxic effects of harmful benthic dinoflagellate *Ostreopsis ovata* on invertebrate and vertebrate marine organisms. Mar. Environ. Res. 76, 97–107.
Falugi, C., Lammerding-Koppel, M., Aluigi, M.G., 2008. Sea urchin development: an alternative model for mechanistic understanding of neurodevelopment and neurotoxicity. Birth Defects Res., C: Embryo Today—Rev. 84, 188–203.
Falugi, C., Aluigi, M.G., Chiantore, M.C., Privitera, D., Ramoino, P., Gatti, M.A., Fabrizi, A., Pinsino, A., Matranga, V., 2012. Toxicity of metal oxide nanoparticles in immune cells of the sea urchin. Mar. Environ. Res. 76, 114–121.
Fenaux, L., Strathmann, M.F., Strathmann, R.A., 1994. Five tests of food-limited growth of larvae in coastal waters by comparisons of rates of development and form of echinoplutei. Limnol. Oceanogr. 39, 84–98.
Fink, R.D., McClay, D.R., 1985. Three cell recognition changes accompany the ingression of sea urchin primary mesenchyme cells. Adv. Dev. Biol. 107, 66–74.
Gambardella, C., Aluigi, M.G., Ferrando, S., Gallus, L., Ramoino, P., Gatti, A.M., Rottigni, M., Falugi, C., 2013. Developmental abnormalities and changes in cholinesterase activity in sea urchin embryos and larvae from sperm exposed to engineered nanoparticles. Aquat. Toxicol. 130–131, 77–85.
Gambardella, C., Gallus, L., Gatti, A.M., Faimali, M., Carbone, S., Vittori Antisari, L., Falugi, C., Ferrando, S., 2014. Toxicity and transfer of metal oxide nanoparticles from microalgae to sea urchin larvae. Chem. Ecol. 30, 308–316.
Guss, K.A., Ettensohn, C.A., 1997. Skeletal morphogenesis in the sea urchin embryo: regulation of primary mesenchyme gene expression and skeletal rod growth by ectoderm-derived cues. Development 124, 1899–1908.
Huang, M., Ma, Z., Khor, E., Lim, L.Y., 2002. Uptake of FITC-chitosan nanoparticles by A549 cells. Pharmacol. Res. 19, 1488–1494.
Jasny, B.R., Prunell, B.A., 2006. The glorious sea urchin—introduction. Science 314, 938.
Johansson, S., Svineng, G., Wennerberg, K., Armulik, A., Lohikangas, L., 1997. Fibronectin–integrin interactions. Front. Biosci. 2, 126–146.
Karlsson, A., 1999. Wheat germ agglutinin induces NADPH-oxidase activity in human neutrophils by interaction with mobilizable receptors. Infect. Immunol. 67, 3461–3468.
Katow, H., Yazawa, S., Sofuku, S., 1990. A fibronectin-related synthetic peptide, Pro-Ala-Ser-Ser, inhibits fibronectin binding to the cell surface, fibronectin-promoted cell migration in vitro, and cell migration in vivo. Exp. Cell. Res. 190, 17–24.
Katow, H., Hayashi, M., 1985. Role of fibronectin in primary mesenchyme cell migration in the sea urchin. J. Cell Biol. 101, 1487–1491.
Kobayashi, N., 1991. Marine pollution bioassay by using sea urchin eggs in the Tanabe bay, Wakayama prefecture, Japan, 1970–1987. Mar. Pollut. Bull. 23, 709–713.
Kou, L., Sun, J., Zhai, Y., He, Z., 2013. The endocytosis and intracellular fate of nanomedicines: implication for rational design. Asian J. Pharm. Sci. 8, 1–10.
Laemmli, U.K., 1970. Cleavage of structural proteins during the assembly of the head of bacteriophage T4. Nature 227 (5259), 680–685.
Leaf, D.S., Anstrom, J.A., Chin, J.E., Harkey, M.A., Raff, R.A., 1987. Antibodies to a fusion protein identify a cDNA clone encoding msp130, a primary mesenchyme-specific cell surface protein of the sea urchin embryo. Adv. Dev. Biol. 121, 29–40.
Lennett, E.D.A., 1978. An improved mounting medium for immunofluorescence microscopy. Am. J. Clin. Pathol. 69, 647–648.
Mann, K., Wilt, F.H., Poustka, A.J., 2010. Proteomic analysis of sea urchin (*Strongylocentrotus purpuratus*) spicule matrix. Proteome Sci. 8, 33.
Manno, D., Carata, E., Tenuzzo, B.A., Panzarini, E., Buccolieri, A., Filippo, E., Rossi, M., Serra, A., Dini, L., 2012. High ordered biomineralization induced by carbon nanoparticles in the sea urchin *Paracentrotus lividus*. Nanotechnology 23, 495104.
Manzo, S., Miglietta, M.L., Rametta, G., Buono, S., Di Francia, G., 2013. Embryotoxicity and spermiotoxicity of nanosized ZnO for Mediterranean sea urchin *Paracentrotus lividus*. J. Hazard. Mater. 15, 254–255.
Martin, S., Richier, S., Pedrotti, M.L., Dupont, S., Castejon, C., Gerakis, Y., Kerros, M.E., Oberhänsli, F., Teyssié, J-L., Jeffree, R., Gattuso, J.P., 2011. Early development and molecular plasticity in the Mediterranean sea urchin *Paracentrotus lividus* exposed to CO_2-driven acidification. J. Exp. Biol. 214, 1357–1368.
Matranga, V., Corsi, I., 2012. Toxic effects of engineered nanoparticles in the marine environment: model organisms and molecular approaches. Mar. Environ. Res. 76, 32–40.
McClay, D.R., Cannon, G.W., Wessel, G.M., Fink, R.D., Marchase, R.B., 1983. Patterns of antigenic expression in early sea urchin development. In: Jeffrey, W.R., Raff, R.A. (Eds.), Time, Space, and Pattern in Embryonic Development. Alan R. Liss, New York, NY, pp. 157–169.
McClay, D.R., Peterson, R.E., Range, R.C., Winter-Vann, A.M., Ferkowicz, M.J., 2000. A micromere induction signal is activated by β-catenin and acts through Notch to initiate specification of secondary mesenchyme cells in the sea urchin embryo. Development 127, 5113–5122.
Miller, J., Fraser, S.E., McClay, D.R., 1995. Dynamics of thin filopodia during sea urchin gastrulation. Development 121, 2501–2511.
Okazaki, K., 1975. Spicule formation by isolated micromeres of the sea urchin embryo. Am. Zool. 15, 567–581.
Pesando, D., Huitorel, P., Dolcini, V., Angelini, C., Guidetti, P., Falugi, C., 2003. Biological targets of neurotoxic pesticides analysed by alteration of developmental events in the Mediterranean sea urchin, *Paracentrotus lividus*. Mar. Environ. Res. 55, 39–57.
Pinsino, A., Della Torre, C., Sammarini, V., Bonaventura, R., Amato, E., Matranga, V., 2008. Sea urchin coelomocytes as a novel cellular biosensor of environmental stress: a field study in the Tremiti Island Marine Protected Area, Southern Adriatic Sea, Italy. Cell. Biol. Toxicol. 24, 541–552.
Privitera, D., Giussani, V., Isola, G., Faimali, M., Piazza, V., Garaventa, F., Asnaghi, V., Cantamessa, E., Cattaneo-Vietti, R., Chiantore, M.C., 2012. Toxic effects of *Ostreopsis ovata* on larvae and juveniles of *Paracentrotus lividus*. Harmful Algae 18, 16–23.
Qiao, D., Nikitina, L.A., Buznikov, G.A., Lauder, J.M., Seilder, F.J., Slotkin, T.A., 2003. The sea urchin embryo as a model for mammalian developmental neurotoxicity: ontogenesis of the high-affinity choline transporter and its role in cholinergic trophic activity. Environ. Health Perspect. 111, 1730–1735.
Ramoino, P., 1997. Lectin-binding glycoconjugates in *Paramecium primaurelia*: changes with cellular age and starvation. Histochem. Cell Biol. 107, 321–329.
Siller, L., Lemloh, M.-L., Piticharoenphun, S., Mendis, B.G., Horrocks, B.R., Brümmer, F., Medakovi, D., 2013. Silver nanoparticle toxicity in sea urchin *Paracentrotus lividus*. Environ. Pollut. 178, 498–502.
Spiegel, E., Burger, M., Spiegel, M., 1980. Fibronectin in the developing sea urchin embryo. J. Cell Biol. 87, 309–313.
Susan, J.M., Just, M.L., Lennarz, J.L., 2000. Cloning and characterization of aP integrin in embryos of the sea urchin *Strongylocentrotus purpuratus*. Biochem. Biophys. Res. Commun. 272, 929–935.
Tyrode, M.V., 1910. The mode of action of some purgative salts. Arch. Int. Pharmacodyn. 20, 205–223.
US Environmental Protection Agency (USEPA), 2002. Methods for Measuring the Acute Toxicity of Effluents and Receiving Waters to Freshwater and Marine Organisms. EPA, Washington, DC (EPA 821-R-02-012).
Wilt, F.H., 1999. Matrix and mineral in the sea urchin larval skeleton. J. Struct. Biol. 126, 216–226.
Wilt, F.H., 2005. Developmental biology meets materials science: morphogenesis of biomineralized structures. Adv. Dev. Biol. 280, 15–25.
Yajima, M., Kijimoto, M., 2006. Study of larval and adult skeletogenic cells in developing sea urchin larvae. Biol. Bull. 211, 183–192.
Zuykov, M., Pelletier, M., Belzile, C., Demers, S., 2011. Alteration of shell nacre micromorphology in blue mussel *Mytilus edulis* after exposure to free-ionic silver and silver nanoparticles. Chemosphere 84, 701–706.